Digest Journal of Nanomaterials and Biostructures Vol. 9, No. 3, July - September 2014, p. 987 - 995

NANOSTRUCTURES WITH IRON OXIDES CORE APPLIED FOR WATER TREATMENT

A. M. PREDESCU[a], E. MATEI[a], D. SAVASTRU[b*], G. COMAN[a], C. PREDESCU[a], G. VLAD[c], L. FAVIER[d]
[a]*Politehnica University of Bucharest, 313 Splaiul Independentei, Bucharest, Romania*
[b]*National Institute of R&D for Optoelectronics INOE 2000, 409 Atomistilor st., Magurele, Romania*
[c]*ICPE Bistrita, 7 Parcului Street, Bistrita , Romania*
[d]*Ecole Nationale Supérieure de Chimie de Renne, 11 Allée de Beaulieu, Rennes,France*

The objective of this work was to establish a correlation between stability of some magnetic iron oxides as nanocrystalline materials and theirs dissolution capacity in different aqueous media. The dimensions of the products were established by morphological and structural characterization with X-ray diffraction (XRD) and transmission electron microscopy (TEM). Concentration of dissolved iron was established with atomic absorption spectrometry (AAS). Results regarding the stability in different media of some magnetic nanostructures were evaluated using the following parameters: maximum quantity dissolved, time of dissolution, pH value of aqueous media. The stability was tested during 24 hours, in order to identify the best compatibility with aqueous media taking into account the real pH values of waters with variable values from acidic to basic pH values. Results indicate a high dissolution tendency under acidic conditions, especially for iron oxides in comparison with bimetallic oxides. The separation from the aqueous media was made by an external magnetically field, due theirs super-paramagnetically behavior. The tendency of dissolution for these types of nanostructurated materials represent the main step in choosing the right pH value of media where these particles can be used.

(Received June 3, 2014; Accepted July 21, 2014)

Keywords: Nanomaterials, Characterization, Stability tests

1. Introduction

Nano-sized magnetic particles are receiving increased attention, in part from the development of high density magnetic storage media, their low cost, tunable electrical and magnetic properties, and excellent phase stability [1].

The high surface area to mass ratios of nanoparticles can greatly enhance the adsorption capacities of sorbent materials [2]. In addition to having high specific surface areas, nanoparticles also have unique adsorption properties due to different distributions of reactive surface sites and disordered surface regions.

Nanoparticles have two key properties that make them particularly attractive as sorbents. On a mass basis, they have much larger surface areas than bulk particles. Nanoparticles can also be functionalized with various chemical groups to increase their affinity towards target compounds. It has been found that the unique properties of nanoparticles to develop high capacity and selective

* Corresponding author: dsavas@inoe.ro

sorbents for metal ions and anions [3]. Characterization of the interactions of the nanoparticles with the bacteria by atomic force microscopy (AFM), Transmission Electron Microscopy (TEM) and laser confocal microscopy showed considerable changes in the integrity of the cell membranes, resulting in the death of the bacteria in most cases. Phototalytic nanomaterials allow ultraviolet light also used to destroy pesticides, industrial solvents and germs [4].

The smaller size of magnetic nanoparticles, which are 2-3 orders of magnitude smaller than a bacterium, provides extra benefits compared to magnetic beads. When their surface is appropriately elaborated, magnetic nanoparticles can also provide efficient binding to the bacteria because their high surface/volume ratio simply offers more contact area. Ferrite is a generic term for a class of magnetic iron oxide compounds [2]. Ferrites posse the property of spontaneous magnetization and are crystalline materials soluble in strong acid. Iron atoms in iron ferrite (FeO.Fe2O3) can be replaced by many other metal ions without seriously altering its spinel structure. Various ferrites and natural magnetite were used in batch modes for actinide and heavy metal removal from wastewater [2]. For example, replacement of a Fe atom with Zn can lead to composite hollow nanospheres as $ZnFe_2O_4$/α-Fe_2O_3 which shows attractive light absorption property for potential applications in electronics, optics, and catalysis [5]. Also, zinc oxide nanostructures are widely used for industrial and biomedical applications [6] and obtaining of a nano-composite based on ferrite structures enhance these properties. Also, nano-silver coated filters were evaluated for antibacterial efficiency [7] and combination between advanced features of nano-Ag and magnetic nanoparticles, as core–hollow–shell nanostructures with Ag nanoparticles as cores and iron oxide as shells resulted in a multifunctional platform for detection and elimination of pathogens [8].

In this paper, three types of magnetic ferrite nanoparticles, magnetite Fe_3O_4, zinc ferrite $ZnFe_2O_3$, silver coated ferrite Ag-Fe_2O_3 were prepared and characterized in order to establish their stability into different aqueous media.

2. Experimental

2.1 Preparation and characterization

Magnetite nanoparticles, Fe_3O_4 were prepared by coprecipitation method as it is described in another paper [9]. All reagents were pure analytical grade (Merck). Zinc ferrite, $ZnFe_2O_4$, was prepared according to Yeary et al., (2011) by slowly adding a 40% NaOH solution into a mixed solution of total 0.2 M of $FeCl_3 \cdot 6H_2O$ and 0.1 M $ZnCl_2$ solution until pH 7 with rapid stirring. The precipitates were washed three times with deionized water, precipitates were centrifuged each time, and deionized water was added to make the final precursor suspension.

Silver ferrite composite was prepared according to Murthy et al., [10] using a mixture of 0.05M silver nitrate and 0.05M ferric nitrate solutions in double distilled and de-ionized water was stirred for 4h at 27 °C, and then heated to 70 °C for 1h. 0.4M (25ml) solution of sodium hydroxide was prepared and slowly added to the above solution by monitoring the pH of the solution. The reactants were constantly stirred by a magnetic stirrer until a pH level of 11–12 was reached. The stirring was further continued for 6 h for aging. The resulting ruby-brown precipitate was collected by filtration and washed with de-ionized water for several times and then dried. The resulting powders are found to be of rich by red color. These powders were annealed at 400, 700 and 900 °C and subjected to XRD studies to characterize the structure and determine the grain size.

The materials were characterized by X-ray diffraction (XRD) and scanning electron microscopy (SEM) coupled with energy dispersive X-ray spectra (EDS) methods. A Panalytical X'Pert PRO MPD X-ray diffractometer with high-intensity Cu–Kα radiation (λ = 1.54065 A) and 2θ range from 10 to 90° was used to obtain XRD patterns. To evaluate the average dimension of the crystallites, the Debye–Scherrer Eq. 1 was used [11, 12]:

$$D = \frac{K x \lambda_{Cu-K\alpha}}{\cos\theta x FWHM} \quad (1)$$

where: D – crystallite dimension; K – coefficient (0.89); λCu-Kα - the wavelength of the radiation for diffraction tube; FWHM - Full width at half maximum of diffraction, in the 2θ scale (in radians); θ - Diffraction Bragg angle.

The SEM investigations were performed on a Quanta INSPECT F scanning electron microscope equipped with a field emission gun at a resolution of 1.2 nm and EDS with a resolution for Mn–Kα of 133 eV. Investigation of samples were performed by using of a Quanta INSPECT F scanning electron microscope (SEM) equipped with field emission gun (FEG) with a resolution of 1.2 nm and an energy dispersive X -ray spectrometer (EDXS) with the resolution for MnKα of 133 eV [10].

2.2 Stability tests

In order to evaluate the stability of the three magnetic oxides nanostructures, different pH values of the aqueous media were used. Hydrochloric acid (HCl 0.1 M) and sodium hydroxide (NaOH 0.1M) were added together with magnetic oxide nanostructures and concentration of dissolved iron, zinc and silver was evaluated.

The pH media were 2.5, 6.5 and 8.5, respectively. Contact time was between 10 minutes and 120 minutes and separation of solid material was magnetically, after stirring [13]. The supernatant from aqueous solutions was analyzed by flame atomic absorption spectrometry (FAAS). Determinations were made at 248.3 nm for iron, 328.1 nm for silver and 213.9 nm for zinc with FAAS type GBC 932 AB Plus, lamp current 12.5 mA, spectral bandwidth of 0.2 nm.

The analyses were made in order to establish the leached quantity of total iron, zinc and silver resulted by dissolution under different media.

Each analyzed metal had 3 replicates and the values used to calculate the removal efficiency are represented as the average values.

3. Results

3.1. Preparation and characterization of magnetite (Fe_3O_4) nanoparticles

The crystalline structure of the Fe_3O_4 powder was identified with XRD as it can be seen in Fig. 1, with maximum intensity of peak diffraction at 35.44° for 2θ. The XRD pattern shows a spinel structure for Fe_3O_4, according to 75-1610 ICDD file.

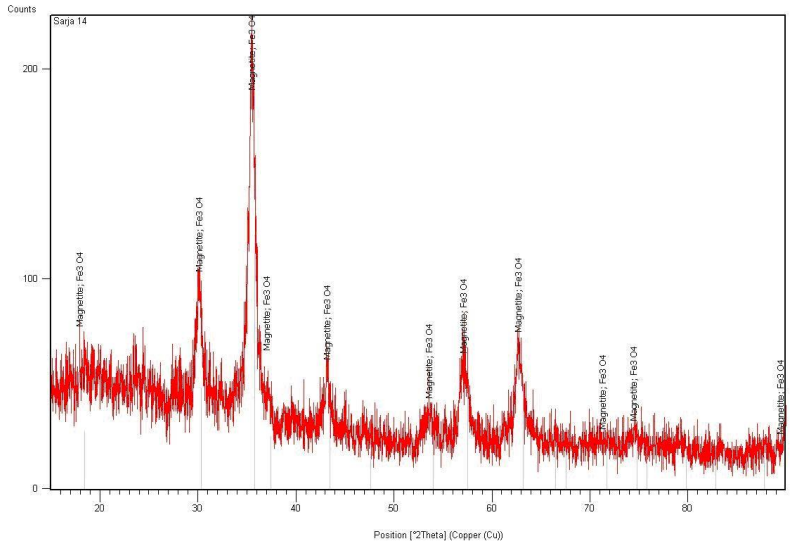

Fig. 1. XRD patterns (CuK_α radiation) for Fe_3O_4

The Debye-Scherrer equation by XRD (Eq.[1]) indicated an average size of the crystallites of 8.55 nm. The dimension is confirmed by TEM measurements for size distribution.

The TEM image of Fe_3O_4 nanoparticles from Figure 2 (a) indicates a good dispersion of nanoparticles. The SAED image from Figure 2 (b) confirmed that Fe_3O_4 is single phase.

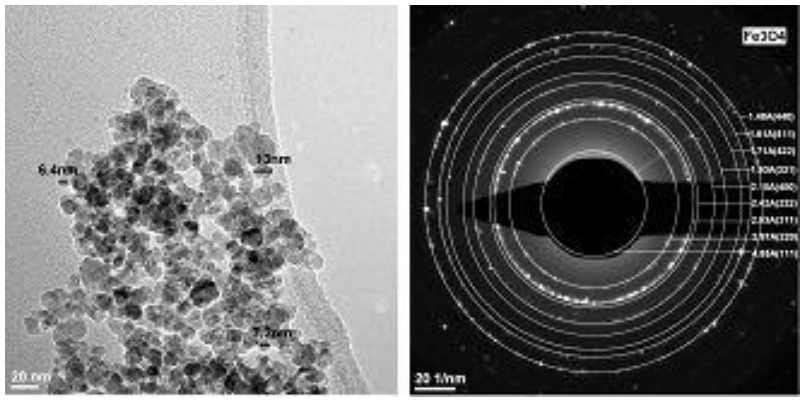

(a) (b)

Fig. 2. TEM image (a) and associated SAED (b) for Fe_3O_4

The average size is 9.45 nm as it can be seen in Figure 3.

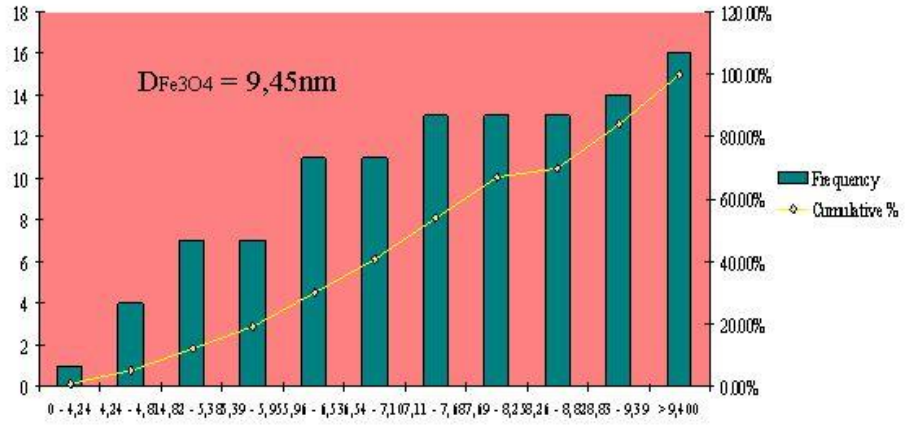

Fig. 3. Dimension distribution for Fe_3O_4 (average size: 9.45 nm)

3.2. Preparation and characterization of zinc ferrite ($ZnFe_2O_4$-Fe_2O_3) nanoparticles

The crystalline structure of the $ZnFe_2O_4$ nanoparticles was identified with XRD as it can be seen in Figure 4, with two maximum intensity of peaks diffraction. First peak for at 2θ appears at 33.134° for rhombohedral system of $\alpha Fe_{1.987}O_3$, specific to hematite according to 77-9927 ICSD file. The second one appears at 36.175° for cubic crystal system of franklinite ($ZnFe_2O_4$) according to 14-7776 ICSD file.

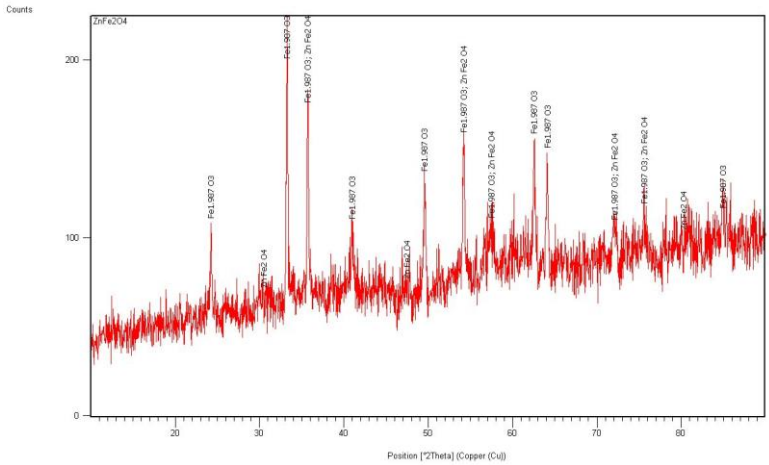

Fig. 4. XRD patterns (CuK$_\alpha$ radiation) for αFe1.987O3 and ZnFe$_2$O$_4$

As it can be seen from the Fig 4, the quantify analysis indicates the presence of $ZnFe_2O_4$ as trace compound at almost 20% in comparison with $\alpha Fe_{1.987}O_3$ as main compound of 80%. This evaluation can be seen in the Fig 5.

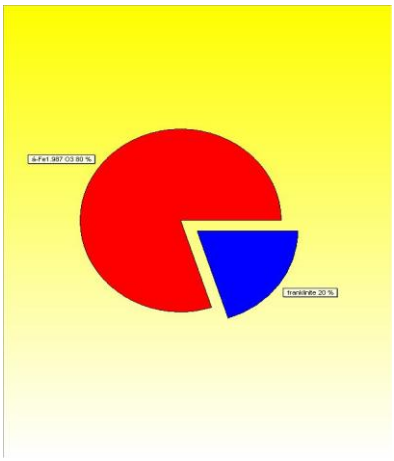

Fig. 5. Quantify analysis with XRD for αFe$_{1.987}$O$_3$ and ZnFe$_2$O$_4$

According to Debye-Scherrer equation (Eq.[1]), the average size of the crystallites was about 16.32 nm for $ZnFe_2O_4$ and 21.28 nm for $\alpha Fe_{1.987}O_3$, respectively.

The SEM images of $ZnFe_2O_4$ nanoparticles from Figure 6 indicate a good dispersion of nanoparticles and specific aspect at 200.000x (a) and 400.000x (b). Energy dispersive spectra (EDS) indicate as single elements Zn and Fe in the sample compositions (c). The presence of oxygen is due the oxides composition.

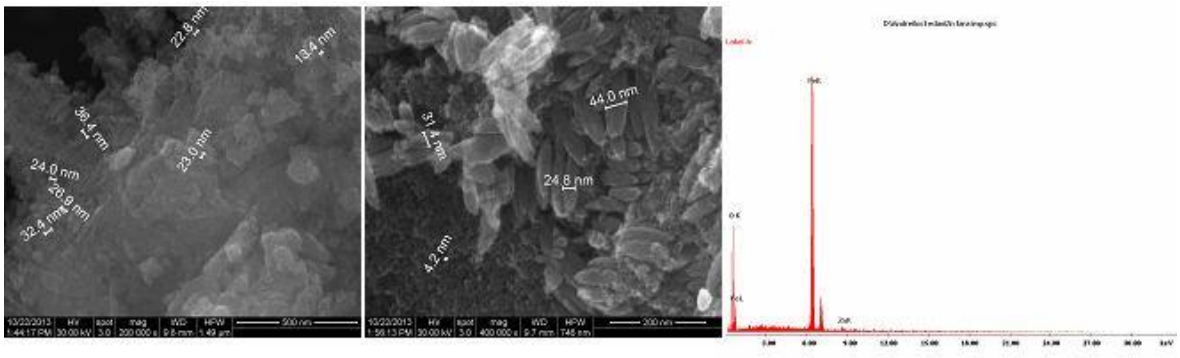

(a) (b) (c)

Fig. 6. SEM image at 200.000 x (a) and 400.000 x (b) associated SAED (c) for $\alpha Fe_{1.987}O_3$ and $ZnFe_2O_4$

3.3. Preparation and characterization of silver ferrite (Ag-Fe_2O_3) nanoparticles

X-ray diffraction (XRD) is shown in Figure 7. A maximum intensity of peak diffraction appears at 38.29° for 2θ associated with cubic crystal system of Ag, according to 71-4612 ISCD file. Also, the XRD pattern shows a rhombohedral structure for hematite as α-Fe_2O_3, according to 2-7501 ICSD file, with maximum peak intensity at 32.977° for 2θ.

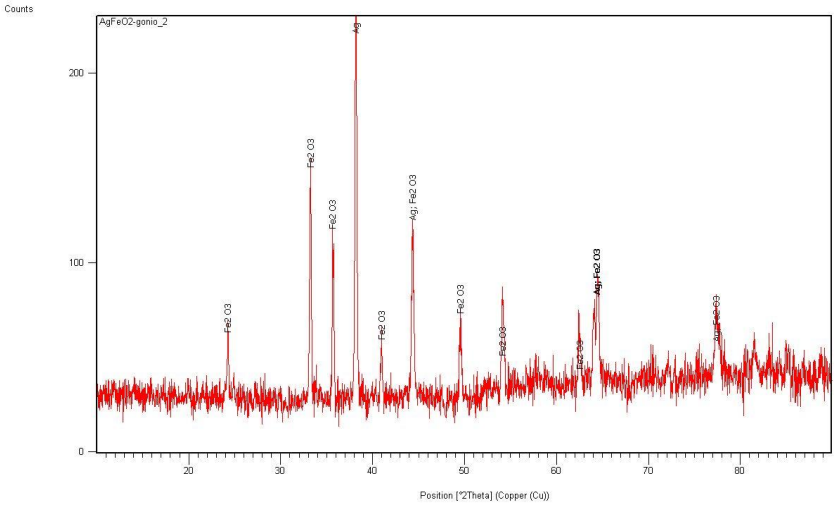

Fig 7. XRD patterns (CuK$_\alpha$ radiation) for silver coated nanoparticles, Ag-Fe_2O_3

The average size of the crystallites was about 15,04 nm for Ag and 19,81 nm for Fe_2O_3, respectively. The dimensions were calculated by Debye-Scherrer equation (Eq.[1]).

The SEM images of nanoparticles from Figure 8 indicate a good dispersion of nanoparticles and specific aspect at 50.000x (a) and 200.000x (b), according to the spherical shape of Ag nanoparticles [14, 15, 16]. Energy dispersive spectra (EDS) indicate as single elements Ag and Fe in the sample compositions (c). The presence of oxygen is due the oxides composition.

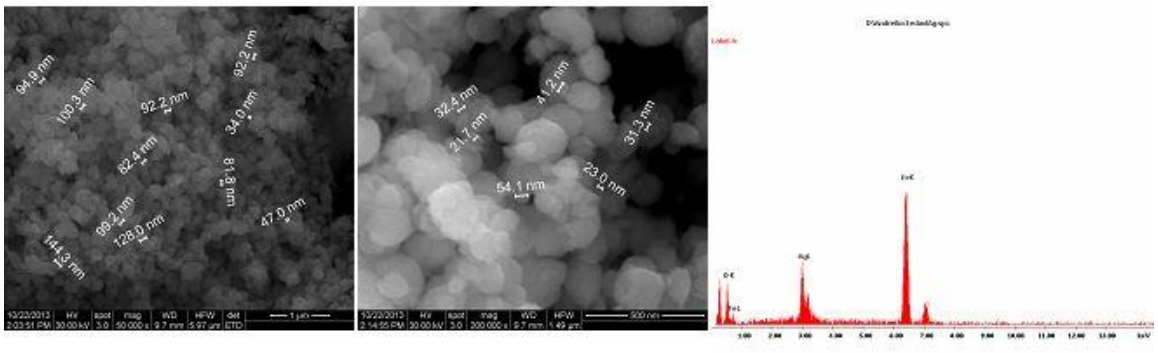

(a) (b) (c)

Fig. 8. SEM image at 200.000 x (a) and 400.000 x (b) associated SAED (c) for $\alpha Fe_{1.987}O_3$ and $ZnFe_2O_4$

3.4. Stability tests

The final application of these compounds represents the waste water treatment, thus the stability was tested under acidic, neutral and basic conditions. The stability tests were made at pH values of 2.5, 6.5 and 8.5, respectively. The tested products were three types of magnetic ferrite nanoparticles, magnetite Fe_3O_4, zinc ferrite $ZnFe_2O_3$, silver coated ferrite Ag-Fe_2O_3.

The initial quantity from each nanomaterial was 1 g which was added at 1000 mL HCl and NaOH, respectively. The total contact time was 120 minutes. The total dissolved metal content, expressed as mg/L was measured with flame atomic absorption spectrometer (FAAS) and the results obtained are shown in Figure 9. The analysis methods were validated under SR ISO CEI 17025/2005 requirements. It can be observed that the most total dissolved iron concentration was obtained under acidic conditions (pH 2.5) for Fe_3O_4, which had the lowest stability.

The high tendency of dissolution was observed under acidic medium (pH 2.5), after 120 minutes, as it is observed in Table 1.

The concentrations were detected for 11 samples from 10 to 10 minutes for each solution and the presented resulted represent average values for 3 replicates. Results are presented in Table 1.

Table 1. The FAAS measurements of the total dissolved iron concentrations, mg/L, at pH 2.5

Time, minutes	Total dissolved metal content, mg/L:				
	Fe_3O_4	$ZnFe_2O_4$-Fe_2O_3		Ag-Fe_2O_3	
	Fe	Fe	Zn	Fe	Ag
10	26.164	15.166	0.96	11.256	0.50
20	22.658	16.687	1.10	12.578	0.55
30	39.105	17.698	1.09	13.505	0.62
40	40.123	20.235	0.95	14.123	0.67
50	42.156	22.698	1.15	15.145	0.69
60	44.362	25.687	1.08	14.962	0.70
70	45.786	26.894	1.14	15.086	0.72
80	48.897	26.842	1.15	16.897	0.76
90	48.654	27.981	1.18	18.654	0.79
100	50.120	28.967	1.20	19.120	0.78
120	49.567	31.287	1.19	19.567	0.81

Also, Zn and Ag dissolution process was evaluated under the same conditions. The rate of dissolution under acidic, neutral and basic conditions is presented in Figure 9.

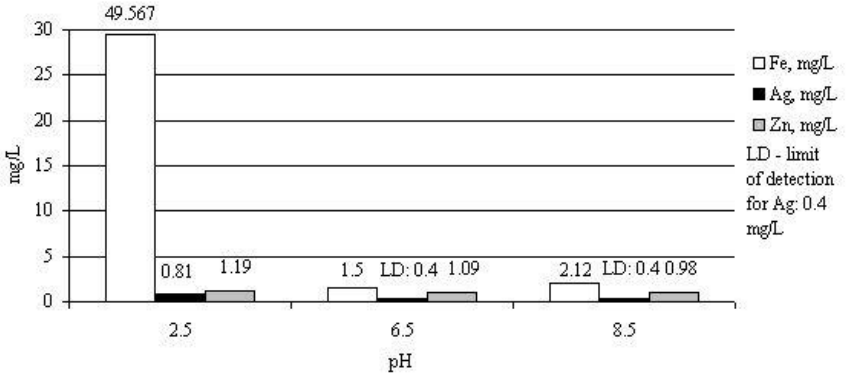

Fig 9. Dissolved metal content at different pH values.

It can be observed that dissolution of Zn was higher than Ag under acidic media after 120 minutes. Under neutral and basic conditions the dissolution appears after 10 minutes and becomes lower after this period, probably to the formation of a hydroxide layer at the ferrite surface, according to Palmer and co-workers [4] which state that in such cases these "binuclear "solid phases are expected to dissolve incongruently, leaving the more soluble component in solution while precipitating the less soluble component as its oxide or hydroxide [17].

Also, it can be observed that dissolved Zn content is almost the same under acidic and basic conditions.

Thus, under acidic conditions (pH 2.5), the tendency of iron dissolution decreases in order: Fe_3O_4 > $ZnFe_2O_4$-Fe_2O_3 > Ag-Fe_2O_3.

The tendency of Ag dissolution could not be evaluated under neutral and basic conditions, these values being under 0.4 mg/L as detection limit of FAAS for Ag analysis. The higher tendency of Zn under acidic, basic and neutral conditions in comparison with Ag is made of coated nanoparticle of $ZnFe_2O_3$ by a layer of $\alpha Fe_{1.987}O_3$.

4. Discussions

In case of Fe3O4, dimensions of the crystallites calculated with Debye-Scherrer formula has the same value as average size calculated by TEM analysis. This indicates that nanoparticles analyzed by TEM are single crystallites identified by XRD. The presence of $ZnFe_2O_4$ as trace compound for the analyzed sample together with αFe_2O_3 indicated formation a nano-composite with cubic $ZnFe_2O_4$ and rhombohedral α-Fe_2O_3 distributed irregularly in one nanosphere. Particle size is several tens of nanometers, which is consistent with the result from the XRD analysis and SEM. Ag analysis confirmed that only ferrite and metallic silver were present in the Ag-Fe_2O_3 nanocomposite.

The tendency of dissolution for the three nano-composites indicates a high capacity of dissolution under acidic conditions, especially for Fe, after 10 minutes. In these conditions, the properties of these nano-composites used for water treatment process can be improved by combining with some polymers in order to increase their stability.

5. Conclusions

Three types of ferrite with nanometric dimensions (magnetite Fe_3O_4 with an average diameter of 9.45 nm, $ZnFe_2O_4$-Fe_2O_3 with dimensions of 16.32 nm for $ZnFe_2O_4$ and 21.28 nm for $\alpha Fe_{1.987}O_3$ and Ag-Fe_2O_3 with dimensions of were synthesized using as methods coprecipitation in order to obtain ferrous oxide nanostructures used for water treatment.

The morphology studies confirmed the presence of synthesized products with a slightly agglomeration tendency. The stability for these nanomaterials was demonstrated by leaching test

application, under different media. The highest stability was confirmed under neutral and basic conditions. Under acidic conditions a high tendency of iron dissolution was observed.

The results of this work are used for assessment the efficiency of these types of nanomaterials in water treatment applications, where these compounds can be used as adsorbents for toxic metal ions, their use as adsorbents being justified by high surface area and reactivity.

Acknowledgements

The work has been funded by the Sectoral Operational Programme Human Resources Development 2007-2013 of the Ministry of European Funds through the Financial Agreement POSDRU/159/1.5/S/132395.

References

[1] L. W. Yeary, J.W. Moon, C. J. Rawn, L. J. Love, A.J. Rondinone, J.R. Thompson, B.C. Chakoumakos, T.J. Phelps, J Magn Magn Mater **323**, 3043 (2011).
[2] K. T. Dhermendra, J. Behari, P. Sen, World Appl. Sci. J. **3**(3), 417 (2008).
[3] A. Xia, C. Jin, D. Du, Y. Sun, L. Tong, J Magn Magn Mater, **323**, 2080 (2011).
[4] D. A. Palmer (retired), Lawrence M. A., Wilson L.L., Proceedings of ICPWS XV (15th Internat. Conference on the Properties of Water and Steam), September 8–11 (2008).
[5] Y. Shen, X. Li, Q. Zhao, Y. Hou, M. Tade, S. Liu, Mater. Res. Bull., **46**(12), 2235 (2011).
[6] A. Spoiala, I.-A. Nedelcu, D. Ficai, A. Ficai, E. Andronescu, Dig J Nanomater Bios, **8**(3), 1235 (2013).
[7] F. Heidarpour, W.A.W.A.K. Ghani, A. Fakhru'L-Razi, S. Sobri, A. Torabian, V. H Heydarpour, M. Zargar, Dig J Nanomater Bios, **6**(2), 791 (2011).
[8] Z. Wei, Z. Zhou, M. Yang, C. Lin, Z. Zhao, D. Huang, Z. Chen, J. Gao, J.Mater.Chem. **21**, 16344 (2011).
[9] E. Matei, A. M. Predescu, C. Predescu, M.G. Sohaciu, A. Berbecaru, C. I. Covaliu, J Environ Qual , **42** (1) , 129 (2012).
[10] Y.L.N. Murthy, R.T. Kondala, I.V. Kasiviswanath, R. Singh, J Magn Magn Mater, **322**, 2071 (2010).
[11] F. Miculescu, G.E. Stan, L.T. Ciocan, M. Miculescu, A. Berbecaru, I. Antoniac, Dig J Nanomater Bios, **7**(4), 1667 (2012).
[12] A. Milev, M. Wilson, G.S.K. Kannangara, N. Tran, Mater. Chem. Phys **111**(2–3), 346 (2008).
[13] E. Matei, C. Predescu, A. Berbecaru, A. Predescu, R. Trusca, Dig J Nanomater Bios , **6**(4), 1701 (2011).
[14] M. R. Al-Othman, A.R.M. Abd El-Aziz, M.A. Mahmoud, S.A. Eifan, M.S. El-Shikh, M. Majrashi, Dig J Nanomater Bios, **9**(1), 151 (2014).
[15] O. Monnereau, L. Tortet, CEA Grigorescu, D. Savastru, CR Iordanescu, F. Guinneton, R. Notonier, A. Tonetto, T. Zhang, IN Mihailescu, D. Stanoi, HJ Trodahl, J Optoelectron Adv Mater¸ **12**(8), 1752 (2010).
[16] C. Predescu, N. Ghiban, M. Sohaciu, D. Savastru, E. Matei, A. Predescu, A. Berbecaru, G. Coman, Optoelectron Adv Mater - Rapid Communications, **8**(1-2), 149 (2014).
[17] M.I. Rusu, R. Zamfir, E. Ristici, D. Savastru, C. Talianu, S. Zamfir, A. Molagic, C. Cotrut, J Optoelectron Adv Mater, **8**(1), 230 (2006).